2013

Higgs decays as a window into the dark sector

Hooman Davoudiasl

Hye-Sung Lee

Ian Lewis

Hye-Sung Lee
William & Mary

Recommended Citation

Davoudiasl, H., Lee, H. S., Lewis, I., & Marciano, W. J. (2013). Higgs decays as a window into the dark sector. Physical Review D, 88(1), 015022.

PHYSICAL REVIEW D **88,** 015022 (2013)

Higgs decays as a window into the dark sector

Hooman Davoudiasl,[1] Hye-Sung Lee,[1,2,3] Ian Lewis,[1] and William J. Marciano[1]

[1]*Department of Physics, Brookhaven National Laboratory, Upton, New York 11973, USA*
[2]*Department of Physics, College of William and Mary, Williamsburg, Virginia 23187, USA*
[3]*Theory Center, Jefferson Lab, Newport News, Virginia 23606, USA*

(Received 29 April 2013; published 16 July 2013)

A light vector boson, Z_d, associated with a "dark sector" $U(1)_d$ gauge group has been introduced to explain certain astrophysical observations as well as low energy laboratory anomalies. In such models, the Higgs boson may decay into $X + Z_d$, where $X = Z$, Z_d or γ. Here, we provide estimates of those decay rates as functions of the Z_d coupling through either mass mixing (e.g., via an enlarged Higgs mechanism) or through heavy new fermion loops and examine the implied LHC phenomenology. Our studies focus on the higher m_{Z_d} case, $\gtrsim$ several GeV, where the rates are potentially measurable at the LHC, for interesting regions of parameter spaces, at a level complementary to low energy experimental searches for the Z_d. We also show how measurement of the Z_d polarization (longitudinal vs transverse) can be used to distinguish the physics underlying these rare decays.

DOI: 10.1103/PhysRevD.88.015022 PACS numbers: 12.60.−i, 14.80.Bn, 14.70.Pw, 13.85.−t

I. INTRODUCTION

The discovery of a 125–126 GeV scalar state at the LHC [1,2] appears to have provided the last missing ingredient, namely, the Higgs boson, of the very successful Standard Model (SM) of particle physics. Given its important connection to the generation of elementary particle masses, the new state, henceforth referred to as the Higgs and denoted by H, is potentially a good place to look for physics beyond the SM. For example, $H \to \gamma\gamma$ can deviate from the SM expectation [3,4] if new weak scale states contribute to the loop processes that mediate the decay. Early hints of such a deviation may already be present. However, further analysis and more data are necessary to address this question, as the current experimental situation does not allow one to draw definite conclusions [5].

In any event, since the SM is insufficient to explain all observations of nature, additional new physics is still required and one can expect more measurements of the Higgs could provide additional surprises. For example, the presence of dark matter (DM), accounting for more than 80% of the matter in the Universe [6], is as-of-yet unexplained.

On general grounds, one may expect that the DM is part of a larger particle sector whose interactions with the visible matter (SM) are not completely decoupled. Such a point of view has been adopted in explaining some astrophysical data that could be interpreted as DM signals. For examples, see Refs. [7–9] for an explanation of the 511 keV gamma rays observed by Integral/SPI [10] and Ref. [11] for an explanation of the electron and positron excesses observed by ATIC [12] and PAMELA [13]. Independent of DM considerations, there are also other possible clues that point to the presence of new physics, in particular the 3.6σ discrepancy between the measured value of the muon anomalous magnetic moment $g_\mu - 2$ and its predicted value in the SM [6,14,15]. This and other tentative, less significant hints of beyond the SM physics may also potentially originate from the same "dark sector" that includes DM.

In light of the above considerations, we examine here how a $U(1)_d$ gauge interaction in the "dark" or "hidden" sector may manifest itself in Higgs decays. In particular, we consider the possibility that this Abelian symmetry is broken, giving rise to a relatively light vector boson Z_d with mass $m_{Z_d} \lesssim 10$ GeV. We further assume that Z_d, being a hidden sector state, does not couple to any of the SM particles including the Higgs directly, i.e. SM particles do not carry dark charges. We do allow for the possibility of particles in extensions of the SM, such as a second Higgs doublet or new heavy leptons, to carry dark charges, leading to indirect couplings, via Z-Z_d mixing or loop-induced interactions. This allows us to assume that the properties of H are close to those of the SM Higgs, as the current experimental evidence seems to suggest. For simplicity we will ignore the possibility of H mixing with other scalars unless specified otherwise.

We will consider decays of the type

$$H \to X Z_d \qquad (\text{with } X = Z, Z_d, \gamma) \tag{1}$$

and examine the prospects for detecting such signals at the LHC with emphasis on the $H \to Z Z_d$ decay mode. Other possibilities will only be briefly commented on.

II. FORMALISM AND PHENOMENOLOGY

Quite generally, there are two classes of operators that contribute to the H decays of interest in our work: (A) dimension-3 and (B) dimension-5 operators.

A. Dimension-3 operators

We have,[1,2]

$$O_{A,X} = c_{A,X} H X_\mu Z_d^\mu, \tag{2}$$

with $c_{A,X}$ a coefficient that has mass dimension $+1$. By gauge invariance $X \neq \gamma$ in this case. This kind of operator typically arises from mass mixing between the SM Z and Z_d or by Higgs mixing with another scalar, such as a second Higgs doublet, that carries $U(1)_d$ charge and gets a vacuum expectation value. [See Fig. 1(a).] For a discussion of the latter possibility see, e.g., Ref. [17] where Higgs mixing with a SM singlet scalar charged under $U(1)_d$ has been considered. Whatever its origin, for processes mediated by the operator $O_{A,X}$, the boosted Z_d final states will be primarily longitudinal.

When a mass mixing is involved, it is straightforward to understand the manifest longitudinal polarization. The longitudinal polarization of the physical eigenstate Z_d inherits a component of a SM Nambu-Goldstone boson (NGB) from the SM Z. Hence, for a high energy longitudinally polarized Z_d, we can make the replacement in Eq. (2):

$$Z_d^\mu \to \partial^\mu \phi / m_{Z_d} + \mathcal{O}(m_{Z_d}/E_{Z_d}), \tag{3}$$

where ϕ is a NGB and E_{Z_d} is the energy of the Z_d. Hence, when the Z_d is highly boosted, the longitudinal mode is enhanced over the transverse polarizations by the energy dependence of the derivative coupling of the NGB.

For operators of type $O_{A,X}$ in Eq. (2), we will focus on $X = Z$. Such interactions are typically associated with mixing. For example, the mass term for Z-Z_d mixing can be parametrized as $\varepsilon_Z m_Z^2 Z Z_d$, with

$$\varepsilon_Z = \frac{m_{Z_d}}{m_Z}\delta, \tag{4}$$

where δ is a model dependent parameter. (We will assume that Z_d is light compared to Z in this work.) The vector boson Z_d couples to the weak neutral current, like the SM Z boson, with a coupling suppressed by ε_Z. This coupling can then provide a new source of parity violation [18] and couplings of Z_d to nonconserved currents. At energies $E \gtrsim m_{Z_d}$, the longitudinal Z_d has enhanced couplings of order $(E/m_{Z_d})\varepsilon_Z$ which dominate its weak scale processes, as implied by the Goldstone boson equivalence theorem [19]. Therefore, we expect the Higgs decay $H \to Z Z_d$ mediated by $O_{A,X}$ to be dominated by longitudinal vector bosons. As discussed in Refs. [18,20], this scenario can be constrained by various experiments, both at low and high energies. (See Ref. [21] for a recent review of the relevant low energy parity violation experiments.)

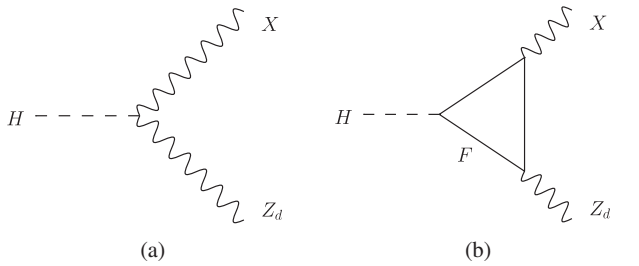

FIG. 1. Processes contributing to interactions for (a) case (A) of the dimension-3 operator (tree-level mixing) and (b) case (B) of the dimension-5 operator (loop-induced decay through a new fermion F).

Roughly speaking, rare B and K decays suggest $\delta^2 \lesssim 10^{-5}$ for $m_{Z_d} \ll 5$ GeV (a scale set by the B meson mass) while the good agreement between precision Z pole property measurements and SM predictions imply $\delta^2 <$ few $\times 10^{-4}$ for all m_{Z_d} [18]. For comparison, the good agreement between early H decay data at the LHC already suggests $\delta^2 \lesssim 10^{-4}$ for some values of m_{Z_d} [18] which is competitive with precision Z pole studies and the (somewhat model dependent) rare meson decays. Hence, continued future searches for $H \to X Z_d$ hold the promise of providing a sensitive, unique probe of Z-Z_d mixing, particularly in the higher m_{Z_d} region above a few GeV where rare flavor decays are not applicable.

We briefly compare the rare Higgs branching ratios for the typical case of Z-Z_d mass mixing. As studied in Ref. [18], we have $\mathrm{Br}(H \to Z Z_d) \simeq 16\delta^2$. For the given bound on δ^2, this branching ratio is possibly comparable to $\mathrm{Br}(H \to \gamma\gamma) \simeq 2.3 \times 10^{-3}$ for the SM Higgs of 125 GeV. The decay $H \to Z_d Z_d$ is negligible, as it is doubly suppressed by δ^2 $(\Gamma(H \to Z_d Z_d)/\Gamma(H \to Z Z_d) \simeq 5\delta^2)$. Finally, there is no $H \to \gamma Z_d$ at leading order.

B. Dimension-5 operators

These operators can be CP even or odd. The CP even interaction has the form

$$O_{B,X} = c_{B,X} H X_{\mu\nu} Z_d^{\mu\nu}, \tag{5}$$

where $X_{\mu\nu} = \partial_\mu X_\nu - \partial_\nu X_\mu$ is the field strength associated with X. The CP odd interaction can be written as

$$\tilde{O}_{B,X} = \frac{\tilde{c}_{B,X}}{2} \varepsilon_{\mu\nu\rho\sigma} H X^{\mu\nu} Z_d^{\rho\sigma}. \tag{6}$$

Here, $c_{B,X}$ and $\tilde{c}_{B,X}$ have mass dimension -1 and are model dependent. Generically, these interactions result from 1-loop processes [see Fig. 1(b)]. For example, in models with vectorlike fermions carrying $SU(2) \times U(1)_Y \times U(1)_d$ quantum numbers such as the heavy lepton model of Ref. [22], these operators can naturally occur.

[1]We will not separately list operators that involve derivatives of the Higgs [16], as they can be recast, using equations of motion, into one of the forms considered below.

[2]Although not explicitly written, here and henceforth for $X = Z_d$, we assume an additional factor of $1/2$ in our operator definitions to account for an additional combinatoric factor of 2 in the Feynman rules for identical particles.

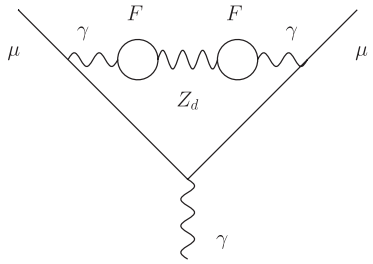

FIG. 2. Z_d contribution to the $g_\mu - 2$. The new fermion (F) loop-induced γ-Z_d mixing is explicitly shown.

The CP odd interaction in Eq. (6) arises if the new fermions have complex couplings to the Higgs that introduce CP violating physical phases [23].

One-loop effects from the aforementioned vector fermions typically result in kinetic mixing between $U(1)_d$ and $U(1)_Y$ [24–26], parametrized by

$$\frac{\varepsilon}{2\cos\theta_W} B_{\mu\nu} Z_d^{\mu\nu}, \tag{7}$$

where θ_W is the weak mixing angle and $B_{\mu\nu}$ is the hypercharge field strength tensor. For a loop-generated ε, we would generally expect $\varepsilon \sim e g_d/(16\pi^2) \sim \mathcal{O}(10^{-3})$ assuming unit charges; e is the electromagnetic coupling constant, and g_d is the $U(1)_d$ gauge coupling. The vector Z_d can couple to the electromagnetic current like a photon with a coupling suppressed by ε.

A light Z_d with small coupling to the electromagnetic current can contribute to the $g_\mu - 2$. The relevant diagram, explicitly showing the γ-Z_d mixing through heavy fermion (F) loops, is given in Fig. 2. A similar loop-induced vertex amplitude is illustrated in Fig. 1(b) for the Higgs decay into Z_d.

The Z_d contribution to $g_\mu - 2$ can explain the current 3.6σ deviation of the muon anomalous magnetic moment from the SM prediction [27,28] in a parameter region indicated by the green band in the $\varepsilon^2 - m_{Z_d}$ parameter space in Fig. 3(a). As the figure shows, roughly $\varepsilon^2 \sim 10^{-6}$–$10^{-5}$ and $m_{Z_d} \sim 20$–50 MeV are left, after various experimental constraints with the most recently updated values are imposed: electron $g - 2$ [22,29], beam dump experiments [30,31], meson decays into Z_d (Υ decays at $BABAR$ [30], ϕ decays at KLOE [32], π^0 decays at SINDRUM [33,34] and WASA-at-COSY [35]), and fixed target experiments (MAMI [36], APEX [37]). The requisite value of ε for the $g_\mu - 2$ explanation can naturally arise from 1-loop diagrams if $g_d \approx e$. Figure 3(b) shows the expected sensitivities of future Z_d searches beyond existing bounds in the same parameter space [38].

As we discussed, the low mass region ($m_{Z_d} \lesssim 1$ GeV) is particularly well motivated by the $g_\mu - 2$ discrepancy but it is being thoroughly explored by direct production at electron facilities (such as the one at Jefferson Lab in the U.S. and the one at Mainz in Germany), as well as rare meson decays. In this paper, we will concentrate on the higher mass region ($m_{Z_d} \gtrsim 1$ GeV) which is potentially accessible in Higgs decays.

Assuming that the couplings in Eqs. (5) and (6) are induced by loops of vectorlike fermions, with $SU(2) \times U(1)_Y$

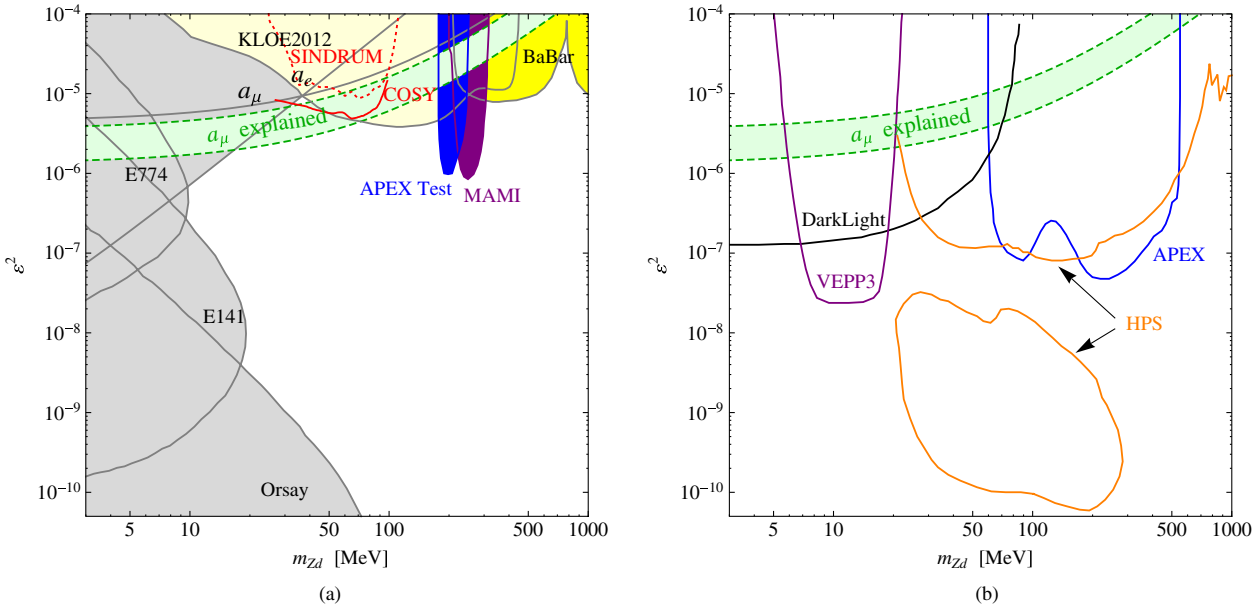

FIG. 3 (color online). (a) Shaded regions of $\varepsilon^2 - m_{Z_d}$ parameter space ruled out by various experimental constraints. The green band shows the parameter region (90% C.L.) that can explain the 3.6σ discrepancy in $g_\mu - 2$ [22]. (b) The same parameter space showing the sensitivity of future direct light Z_d gauge boson searches. Such search constraints generally assume $\mathrm{Br}(Z_d \to \ell^+\ell^-) \simeq 1$. In the case of VEPP3 [68], the anticipated sensitivity is independent of the $\mathrm{Br}(Z_d \to \ell^+\ell^-)$.

preserving masses m_F, we expect $c_{B,X}$, $\tilde{c}_{B,X} \to 0$ as $m_F \to \infty$. The masses of these fermions are shifted after electroweak symmetry breaking, due to their Yukawa interactions with the Higgs. For $m_F \sim$ few $\times$ 100 GeV and Yukawa couplings $y_F \sim 1$, the lightest new fermions can have masses of $\mathcal{O}(m_Z)$,[3] and [for $\mathcal{O}(1)$ phases] we get

$$|c_{B,X}| \sim |\tilde{c}_{B,X}| \sim \frac{g_w g_d y_F}{16\pi^2 m_Z}, \tag{8}$$

with g_w a typical electroweak coupling constant. Such vectorlike fermions [but not necessarily charged under $U(1)_d$] have been recently proposed as a natural solution to the larger than expected diphoton rate in the early Higgs data at the LHC (for some examples, see Refs. [39–49]).

As discussed in Ref. [22], with the additional assumption of being charged under $U(1)_d$, the aforementioned fermions are also well motivated as mediators of the $U(1)_Y$ and $U(1)_d$ kinetic mixing. In this framework, we can estimate the $H \to \gamma Z_d$, $H \to Z Z_d$, and $H \to Z_d Z_d$ rates. For $g_d \approx e$, as motivated by the above discussion of $g_\mu - 2$, and assuming roughly equal values for $c_{B,X}$ and $\tilde{c}_{B,X}$, it is estimated that $0.1\mathrm{Br}(H \to \gamma\gamma) \approx \mathrm{Br}(H \to \gamma Z_d) \approx 2\mathrm{Br}(H \to Z_d Z_d) \approx 10\mathrm{Br}(H \to Z Z_d)$ if the vectorlike fermions are to explain the Higgs to diphoton decay rate at about 1.5 times the SM prediction.[4] The suppression of $\mathrm{Br}(H \to Z Z_d)$ relative to $\mathrm{Br}(H \to Z_d Z_d)$ is due to an additional phase space suppression of having a massive final state particle, and the factor of two between $\mathrm{Br}(H \to \gamma Z_d)$ and $\mathrm{Br}(H \to Z_d Z_d)$ is due to a symmetry factor from identical final states.

Given the preceding discussion, for $\mathrm{Br}(Z_d \to \ell^+\ell^-) > \mathrm{Br}(Z \to \ell^+\ell^-)$, one could expect signals of $H \to X Z_d$ from the interactions in Eqs. (5) and (6) at the LHC, with current or near future levels of statistics. The Z_d can mimic the promptly converted photon ($\gamma \to e^+ e^-$), although the small nonzero mass and a production vertex near the beam can be used to distinguish the new Z_d events.

We also note that the final state Z_d from decays mediated by $O_{B,X}$ and $\tilde{O}_{B,X}$ would be primarily transversely polarized. This can be understood by making the replacement of the longitudinally polarized Z_d in Eq. (3) into operators $O_{B,X}$ and $\tilde{O}_{B,X}$. In this case, the longitudinal polarizations completely decouple up to $\mathcal{O}(m_{Z_d}/E_{Z_d})$. Hence, for a highly boosted Z_d, the transversely polarized Z_d dominates the interactions mediated by $O_{B,X}$ and $\tilde{O}_{B,X}$.

III. PARAMETRIZATION AND SETUP

Models that could give rise to operators $O_{A,X}$, $O_{B,X}$, and $\tilde{O}_{B,X}$ have recently been studied, for example, in Refs. [18,22,23,50]. Here, we briefly explain our parametrization and set up our notation. The general decay widths for each case can be found in our appendix.

Class (A): Regardless of the origin of $O_{A,X}$ (be it mixing between scalars or vectors), following Z-Z_d mixing we will parametrize the interaction in Eq. (2) by

$$c_{A,X} = \frac{g}{\cos\theta_W}\varepsilon_Z m_Z, \tag{9}$$

where g is the $SU(2)_L$ coupling constant.

Class (B): In analogy with $c_{A,X}$, we parametrize the strength of interactions from $O_{B,X}$ and $\tilde{O}_B$ by

$$c_{B,X} = -\frac{g}{2\cos\theta_W}(\kappa_X/m_Z) \tag{10}$$

and

$$\tilde{c}_{B,X} = \frac{g}{2\cos\theta_W}(\tilde{\kappa}_X/m_Z), \tag{11}$$

respectively, where κ_X and $\tilde{\kappa}_X$ are dimensionless model dependent constants. The normalizations have been chosen for ease of notation in our later results.

As previously pointed out, the interactions mediated by class (A) and (B) operators result in final states that are dominated by the longitudinal and transverse polarizations of the vector bosons, respectively. *This effect can be used as a diagnostic probe of the underlying microscopic process to determine whether they result from class (A) or class (B).* The operators $O_{B,X}$ and $\tilde{O}_{B,X}$ can be further disentangled if the angular distribution of the final state particles are considered. For the Higgs to diphoton decay, for example, see Ref. [23].

The decay products of a very light Z_d in the decay chain $H \to Z Z_d \to 4\ell$ are highly collimated and will be difficult to isolate. Also, the decay $H \to Z Z_d \to 4\ell$ can be expected to have already appeared in the $H \to Z Z^* \to 4\ell$ signal, where the Z_d would appear as a peak in the invariant mass distribution of the Z^*. However, ATLAS [51] and CMS [52] both require that $m_{Z^*} > 12$ GeV in their $H \to 4\ell$ analysis. Hence, the mass range we consider in our LHC study is primarily $m_{Z_d} \approx$ 5–10 GeV which is complementary to searches of lighter Z_d in low energy experiments; see Fig. 3. For Z_ds with mass below 5 GeV, the leptons from Z_d decay will be highly collimated. Our examination of Higgs decays to light vector bosons at the LHC is also complementary to studies based on heavy (TeV scale) Z' scenarios (for example, see Refs. [53,54]). Before closing this section, we would like to point out that the size of $\mathrm{Br}(Z_d \to \ell^+\ell^-)$, $\ell = e$, μ, is model dependent.

[3]For unstable fermions with $m_H > m_F \sim \mathcal{O}(m_Z)$, the Higgs decay channel $H \to F F^*$ opens up. Since $m_F + m_{W,Z} > m_H$, the full decay chain proceeds through an off-shell W or Z: $H \to F F^* \to F F_0 W^*/Z^* \to F F_0 f' \bar{f}$, where f, f' are SM fermions and F_0 is either a SM lepton or a new fermion stable on collider time scales. In either case, this is a four-body Higgs decay and is suppressed relative to the dominant SM decay channels. If F is stable, then the decay $H \to F F^*$ is unavailable for this mass.

[4]At leading order, W loops do not contribute to $O_{B,X}$ and $\tilde{O}_{B,X}$ while their contribution is dominant over the fermion loop contributions in the SM $H \to \gamma\gamma$, $Z\gamma$ processes. The $H \to X Z_d$ rates would then likely be comparatively suppressed.

For example, if kinetic mixing between $U(1)_d$ and $U(1)_Y$ ($\varepsilon \neq 0$) dominates, one might expect $\mathrm{Br}(Z_d \to \ell^+\ell^-) \simeq 0.3$ for the 5–10 GeV mass range, while for Z-Z_d mixing dominance, it could be smaller [18]. Because of that arbitrariness, we will give our results in terms of $\delta^2 \times \mathrm{Br}(Z_d \to \ell^+\ell^-)$.

IV. NUMERICAL ANALYSIS

We now present the results of our collider simulation. We study the observability of

$$pp \to H \to ZZ_d \to \ell_1^+\ell_1^-\ell_2^+\ell_2^- \tag{12}$$

at the $\sqrt{s} = 14$ TeV LHC, where ℓ_1 and ℓ_2 are electrons or muons.

The decay $H \to ZZ_d$ is an interesting channel to study as it can arise in both class-(A)—and class-(B)—type interactions. The $H \to \gamma Z_d$ mode is not relevant for class (A), since gauge invariance does not allow it. While the $H \to Z_dZ_d$ decay may also occur for both classes of interactions, it will be doubly suppressed if it results only from Z-Z_d mass mixing. The decay widths for all three modes are presented in the appendix, using the parametrization of the previous section (ε_Z, κ_X, $\tilde{\kappa}_X$).

The region of interest is a relatively light Z_d, and so, unless otherwise noted, we use a Z_d and Higgs mass of

$$m_{Z_d} = 5 \text{ GeV} \quad \text{and} \quad m_H = 125 \text{ GeV}. \tag{13}$$

In our analysis we find that the kinematic cuts affect events from operators of class (A) and (B) somewhat differently. For simplicity, the results of the numerical simulation are presented in detail with the coupling constants

$$\delta^2 \times \mathrm{Br}(Z_d \to \ell^+\ell^-) = 10^{-5} \quad \text{and} \quad \kappa_Z = \tilde{\kappa}_Z = 0. \tag{14}$$

More general cases can be obtained by rescaling the overall coupling and taking into account how the kinematic cuts effect the two classes of events, as is detailed at the end of our analysis.

Using the results of Ref. [18], the above choice corresponds to $\mathrm{Br}(H \to ZZ_d) \approx 2 \times 10^{-4}/\mathrm{Br}(Z_d \to \ell^+\ell^-)$. As mentioned before, when kinetic mixing dominates, the branching ratio of Z_d into leptons is typically given by $\mathrm{Br}(Z_d \to e^+e^-) \simeq \mathrm{Br}(Z_d \to \mu^+\mu^-) \simeq 0.15$.

We now discuss how to isolate our signal from backgrounds. All signal and backgrounds were simulated using MadGraph 5 [55] with the CTEQ6L parton distribution set [56]. The operators in Eqs. (2), (5), and (6), with the parametrization in Eqs. (9)–(11) were implemented into MadGraph 5 using FeynRules [57].

To isolate the signal, it will be useful to implement full event reconstruction. Hence, we need to identify which opposite sign, same flavor lepton pair originates from the Z and which originates from the Z_d. Since both the Z and Z_d have narrow widths, we expect one pair of leptons to reconstruct the Z mass and the other pair the Z_d mass. Since the Z_d mass is not known *a priori*, the Z boson mass is used to identify the decay products. We calculate the invariant mass of all opposite sign, same flavor lepton pairs and identify the pair that closest reconstructs the Z pole as originating from the Z boson. The remaining pair is identified as originating from the Z_d. We will see that the invariant mass distribution of the lepton pair identified as originating from the Z_d will permit a measurement of m_{Z_d}.

Detector resolution effects are simulated via Gaussian energy smearing applied to leptons and jets with a standard deviation parametrized as

$$\frac{\sigma(E)}{E} = \frac{a}{\sqrt{E}} \oplus b, \tag{15}$$

where $\sigma(E)$ is the energy resolution at energy E, $\oplus$ represents addition in quadrature, and all energies are measured in GeV. For leptons (jets) we take the ATLAS values [58] $a = 10\%$ (50%) and $b = 0.7\%$ (3%). The energy resolution of electrons and muons has different dependencies on electromagnetic calorimetry and charged particle tracking. However, we use the uniform values for electromagnetic calorimetry energy resolution for all final state leptons, which, for the energies under consideration, is more conservative than tracking capabilities.

For events to be triggered on, they must pass minimum acceptance cuts on the rapidities, η, and transverse momenta, p_T, of the final state particles. Typically, for leptons a p_T cut around 20 GeV is used. However, for our signal, two of the leptons originate from a low mass resonance and are expected to have low transverse momenta. In Fig. 4, we show the transverse momentum distributions of the hardest (solid) and softest (dashed) leptons identified as originating from the Z (black) and Z_d (red/gray) for the $e^+e^-\mu^+\mu^-$

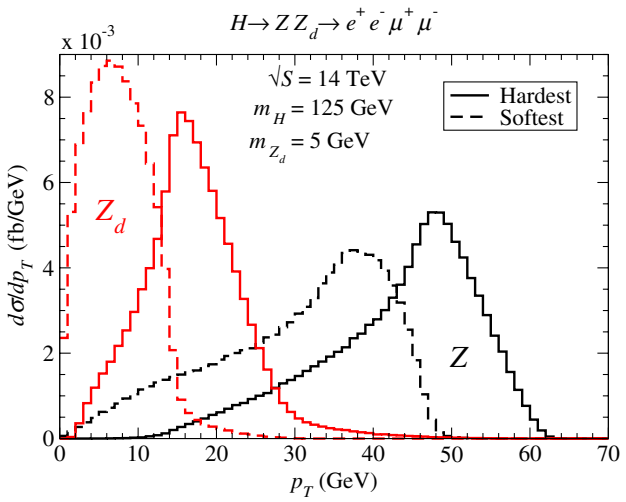

FIG. 4 (color online). Transverse momentum distribution of the hardest (solid) and softest (dashed) leptons identified as originating from the Z (black) and Z_d (red/grey) for the $e^+e^-\mu^+\mu^-$ final state. We use the parameter choices of Eqs. (13) and (14). No energy smearing or cuts have been applied.

TABLE I. Signal and background cross sections (in fb) with consecutive cuts and signal to background ratio S/B after all cuts for the $e^+e^-\mu^+\mu^-$, $2\mu^+2\mu^-$, and $2e^+2e^-$ final states at $\sqrt{s} = 14$ TeV. The parameters in Eqs. (13) and (14) were used.

Channel	$e^+e^-\mu^+\mu^-$		$2\mu^+2\mu^-$		$2e^+2e^-$	
σ (fb)	Signal	Background	Signal	Background	Signal	Background
No cuts and no energy smearing	0.10	⋯	0.051	⋯	0.051	⋯
Basic cuts (16) +Trigger + Isolation. (17)	0.049	67	0.024	26	0.024	26
$+ m_{4\ell}$ (18) $+ m_Z^{\rm rec}$ (19) $+ m_{Z_d}^{\rm rec}$ (23)	0.043	0.030	0.022	0.017	0.022	0.014
S/B	1.5		1.3		1.5	

final state. Distributions for the $2e^+2e^-$ and $2\mu^+2\mu^-$ final states are similar. The leptons from the Z decay are typically harder than those from the Z_d. This can be understood by noting that the momentum of the Z and Z_d in the Higgs rest frame is $|p| \approx 30$ GeV. Hence, the energy of the Z is dominated by the Z mass, m_Z, while the energy of a light Z_d is dominated by $|p|$. The decay products of the Z then have higher transverse momentum than the decay products of the Z_d and typically peak near $m_Z/2$. Based on these considerations, we apply transverse momentum and rapidity cuts on all final state leptons:

$$p_T^\ell > 4 \text{ GeV} \quad \text{and} \quad |\eta^\ell| < 2.5. \tag{16}$$

To trigger on an event, ATLAS and CMS typically require that at least one final state particle have p_T larger than that required by Eq. (16). We follow the ATLAS triggers [1] on $H \to ZZ^* \to 2\ell^+2\ell^-$ events and require that one lepton passes a transverse momentum threshold of 24 GeV or two leptons have a minimum transverse momentum of 13 GeV each.

Signal event characteristics are exploited to develop additional cuts:

(i) To resolve the four leptons of the signal, any pair of leptons is required to satisfy the isolation cut

$$\Delta R = \sqrt{(\Delta\eta)^2 + (\Delta\phi)^2} > 0.3, \tag{17}$$

where $\Delta\eta$ and $\Delta\phi$ are the rapidity and azimuthal angle differences between the two leptons under consideration.

(ii) Since signal events originate from a Higgs boson, the invariant mass of the four leptons should closely reconstruct the Higgs mass. Using typical mass resolutions [1] for a 125 GeV Higgs, the four lepton invariant mass, $m_{4\ell}$, is required to satisfy

$$|m_{4\ell} - m_H| < 2 \text{ GeV}. \tag{18}$$

(iii) Since the Z has a relatively narrow width, the lepton pair identified as originating from the Z should reconstruct m_Z. Hence, we require

$$|m_Z^{\rm rec} - m_Z| < 15 \text{ GeV}, \tag{19}$$

where $m_Z^{\rm rec}$ is the invariant mass of the reconstructed Z boson.

The main backgrounds to our signal consist of the irreducible backgrounds

$$H \to ZZ^*, \qquad Z\gamma^*, \qquad ZZ, \qquad Z(\to 4\ell); \tag{20}$$

the reducible backgrounds Zjj, where the Z decays leptonically and the jets fake leptons; and the $t\bar{t}$ decay chain

$$t\bar{t} \to (b \to c\ell^-)(\bar{b} \to \bar{c}\ell^+)\ell^+\ell^- + \not{p}_T, \tag{21}$$

where $\not{p}_T$ is missing transverse momentum. We assume that a jet fakes an electron or muon 0.1% of the time [2] and use the branching ratio $\mathrm{Br}(b \to c\ell\bar{\nu}) \simeq \mathrm{Br}(B^0 \to \ell\bar{\nu} + \text{anything}) = 0.10$ [6]. Also, the analysis of the $t\bar{t}$ background only takes into consideration the four leptons in the final state, ignoring the missing transverse momentum and extra hadronic activity from the b decays.

The first row of cross sections in Table I shows the signal rate before energy smearing, while in the second row the signal and background rates are given after energy smearing, triggers, and cuts in Eqs. (16) and (17). Background cross sections before minimum cuts are not shown since soft and collinear singularities in some channels do not allow for a reliable estimate. After these cuts, the dominant backgrounds are $t\bar{t}$ and Z, making up ~50% and ~28% of the $e^+e^-\mu^+\mu^-$ background and ~32% and ~38% of the same (lepton) flavor background, respectively. The next largest background is ZZ, contributing ~12% to $e^+e^-\mu^+\mu^-$ and ~26% to same (lepton) flavor backgrounds. Unlike the other backgrounds, which require that at least one same flavor lepton pair originates from a Z, any flavor lepton can originate from a b or W in the top decay. Hence, the different percent contributions to $e^+e^-\mu^+\mu^-$ and same flavor final states for different backgrounds are due to the combinatorics of the $t\bar{t}$ decay into four leptons. The $t\bar{t}$, Z, and ZZ backgrounds are mostly eliminated by the mass cuts in Eqs. (18) and (19), with the large majority of the leftover background coming from $Z\gamma^*$ and $H \to ZZ^*$. (See Fig. 5.)

A. Z_d resonance peak

In Fig. 5, we show the reconstructed Z_d invariant mass, $m_{Z_d}^{\rm rec}$, distribution for major backgrounds (shown cumulatively), and our signal for the $e^+e^-\mu^+\mu^-$ signal after energy smearing, triggers, and cuts in Eqs. (16)–(19). The distribution is similar for the $2e^+2e^-$ and $2\mu^+2\mu^-$

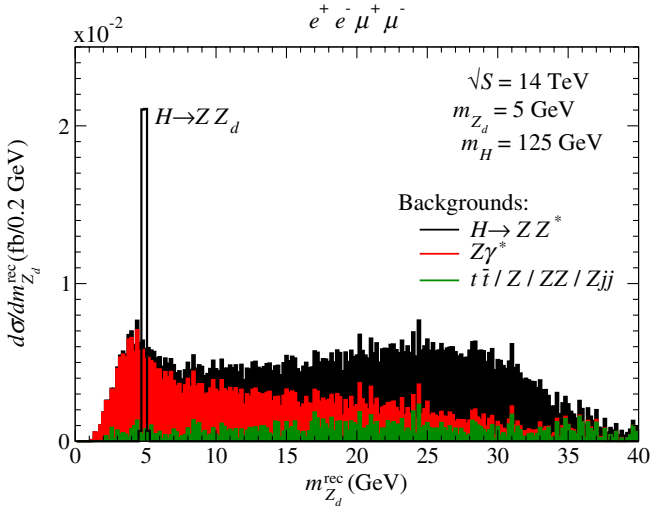

FIG. 5 (color online). Distribution of the reconstructed Z_d invariant mass, $m^{\rm rec}_{Z_d}$, for both major background (shown cumulatively) and signal for the $e^+e^-\mu^+\mu^-$ final state. The parameters of Eqs. (13) and (14) were used. Energy smearing, triggers, and cuts in Eqs. (16)–(19) were applied.

signals. As can be seen, the signal clearly stands out above the background at an invariant mass of $m_{Z_d} = 5$ GeV, and most backgrounds, except $Z\gamma^*$ and $H \to ZZ^*$, are negligible after the mass cuts in Eqs. (18) and (19). The dilepton distributions from $H \to ZZ_d$ and $H \to ZZ^*$ in Fig. 5 show agreement with the results of Ref. [18] which was based on Ref. [59].

The sharp fall in the invariant mass of the background below 5 GeV can be understood by noting the invariant mass of two massless leptons can be written as

$$m_{12}^2 = 2E_1E_2(1 - \cos\theta_{12}), \tag{22}$$

where $E_{1,2}$ and θ_{12} are the energies and angular separation of the two leptons, respectively. Cuts placing a minimum on the energy and the angular separation of the two leptons can be reinterpreted as a minimum on the dilepton invariant mass. The cuts in Eqs. (16) and (17) effectively place a minimum on $m^{\rm rec}_{Z_d}$, as seen in Fig. 5. Hence, to probe Z_d masses below ~4–5 GeV at the LHC, either the isolation or transverse momentum cuts need to be relaxed.

Motivated by Fig. 5, we place the cut on the Z_d reconstructed mass:

$$|m^{\rm rec}_{Z_d} - m_{Z_d}| < 0.1 m_{Z_d}. \tag{23}$$

To illustrate the efficiency of these cuts, Table I lists the cross sections for both signal and background broken down by dilepton final state signals. The second row shows the cross sections after energy smearing, triggers, and cuts in Eqs. (16) and (17), while the third row includes the additional invariant mass cuts of Eqs. (18), (19), and (23). In the last row, we show the signal to background ratio (S/B) after all cuts. As can be clearly seen, the invariant mass cuts leave the signal cross section mostly intact while severely suppressing the backgrounds, and the S/B ratio is well under control.

TABLE II. Luminosities needed for 2σ exclusion, 3σ observation, and 5σ discovery after all cuts for both a $m_{Z_d} = 5$ GeV and $m_{Z_d} = 10$ GeV at $\sqrt{s} = 14$ TeV with and without K-factors. All other parameters are the same as in Eqs. (13) and (14).

	2σ (Exclusion)	3σ (Observation)	5σ (Discovery)
		$m_{Z_d} = 5$ GeV	
No K factors	78 fb^{-1}	180 fb^{-1}	490 fb^{-1}
$+K$ factors	33 fb^{-1}	75 fb^{-1}	210 fb^{-1}
		$m_{Z_d} = 10$ GeV	
No K factors	100 fb^{-1}	230 fb^{-1}	640 fb^{-1}
$+K$ factors	42 fb^{-1}	95 fb^{-1}	260 fb^{-1}

We also explore how sensitive the LHC is to the parameters m_{Z_d} and $\delta^2 \times \mathrm{Br}(Z_d \to \ell^+\ell^-)$. In Table II we illustrate the luminosities needed at $\sqrt{s} = 14$ TeV for 2σ exclusion, 3σ observation, and 5σ discovery for both $m_{Z_d} = 5$ GeV and $m_{Z_d} = 10$ GeV. Significances have been calculated as $S/\sqrt{S+B}$. All other parameters are the same as in Eqs. (13) and (14). For a slightly heavier Z_d, the LHC is found to be less sensitive. The decrease in sensitivity with increasing mass can be understood in part by noting that for a higher m_{Z_d} the cut in Eq. (23) becomes less stringent. For our parametrization the signal rate is the same for both Z_d masses. Since the cumulative background is relatively flat in the region of interest, the amount surviving cuts increases. Hence, the significance slightly decreases as m_{Z_d} increases. Note, however, that the same $\delta^2 \times \mathrm{Br}(Z_d \to \ell^+\ell^-) = 10^{-5}$ was used for both Z_d masses. It is quite plausible, perhaps even likely, that δ is proportional to m_{Z_d}. In that case, the 10 GeV signal will be enhanced by a factor of 4, requiring 6–7 times less than the luminosities listed in Table II.

In Fig. 6, the luminosity needed for a 2σ exclusion (dotted), 3σ observation (dashed), and 5σ discovery (solid) is plotted as a function of $\delta^2 \times \mathrm{Br}(Z_d \to \ell^+\ell^-)$ keeping $m_{Z_d} = 5$ GeV and all other parameters the same as Eqs. (13) and (14). The sensitivity of the LHC dramatically decreases as $\delta^2 \times \mathrm{Br}(Z_d \to \ell^+\ell^-)$ decreases.

The effects considered so far have been at leading order. However, including higher order QCD corrections can increase our sensitivity at the LHC. To approximate these corrections, some standard K factors[5] are applied. The luminosities needed for a 2σ exclusion, 3σ observation, and 5σ discovery after the inclusion of these K factors are shown in Table II. As can be seen, the inclusion of higher

[5] $K \sim 2$ for $gg \to H$ at NNLO-NNLL in α_s [60,61] (N = Next-to; LO = Leading Order; LL = Leading Log), $K = 1.4$ for $t\bar{t}$ at NNLO-NNLL [62], and $K = 1.19$ for Z at NNLO [60,63]. $K = 1.18$ for $Z\gamma$ at NLO in α_s [64,65], $K = 1.62$ for ZZ at NLO [64,66], $K = 0.9$ for Zjj at NLO [67].

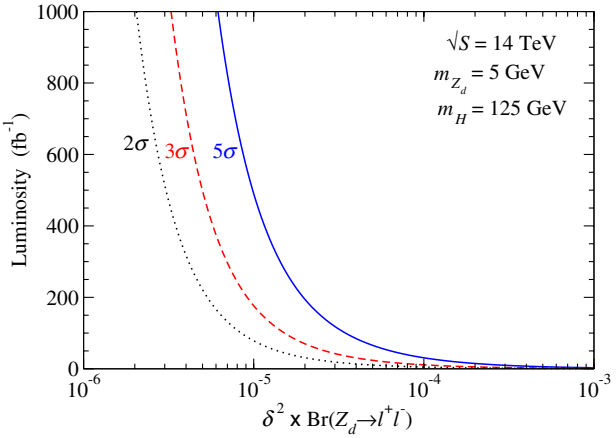

FIG. 6 (color online). Luminosities needed for a 2σ exclusion (dotted), 3σ observation (dashed), and 5σ discovery (solid) as a function of $\delta^2 \times \mathrm{Br}(Z_d \to \ell^+\ell^-)$ at $\sqrt{s} = 14$ TeV. All other parameters are the same as in Eqs. (13) and (14).

order corrections can greatly increase the sensitivity of the LHC to these processes, decreasing the luminosity needed for an observation by roughly 60%.

From Table II and Fig. 6, we conclude that with ~few × 100 fb^{-1} the LHC is sensitive to the four lepton process $H \to ZZ_d$ for Z_d masses in the range 5–10 GeV and can probe $\delta^2 \times \mathrm{Br}(Z_d \to \ell^+\ell^-)$ down to about 10^{-5}. The rescaling of these limits for nonzero κ_X and $\tilde{\kappa}_X$ needs to take into account the effects of the cuts. As discussed in the next section, the transverse momentum cuts in Eq. (16) cut more signal from operators of class (B) than class (A), due to the transverse polarization of the Z_d's. The cuts of Eqs. (16) and (17) and triggers decrease the signal rate of operators of class (A) by ~50% [see Table I] and operators of class (B) by ~65%. These limits can also simply be scaled to generalize to the case with different branching ratios of Z_d into leptons.

B. Angular Distribution

As mentioned earlier, interactions mediated by the operators of class (A) are expected to be dominated by the longitudinal polarizations of the Z_d, while the operators of class (B) are dominated by its transverse polarizations. Once a $H \to ZZ_d$ signal is discovered, determining the polarization of the Z_d can allow us to discriminate whether the interaction is originating from the operators of class (A) or (B).

A good diagnostic of vector boson polarization is the angular distribution of its decay products. In the Z_d rest frame, we have

$$\frac{d\Gamma(Z_d \to \ell^+\ell^-)}{d\cos\theta_\ell} \sim (1 \pm \cos^2\theta_\ell), \tag{24}$$

where θ_ℓ is the lepton (ℓ^-) angle with respect to the Z_d spin-quantization axis, and the upper (lower) sign is for a transversely (longitudinally) polarized Z_d. Events produced via operators of class (A) and class (B) are therefore expected to result in different leptonic angular distributions of the Z_d decay products, allowing for a distinction between the two cases. To exploit this effect, a spin-quantization axis must be chosen such that the Z_d is mostly longitudinally or transversely polarized with respect to that axis.

For $m_{Z_d} \ll m_H - m_Z$, the Z_d will be produced highly boosted and is well approximated as a helicity eigenstate. That is, the Z_d is mostly in a longitudinally or transversely polarized state with respect to its moving direction. One might expect to be able to use the Z_d moving direction as the spin-quantization axis and use the angular distribution of Eq. (24) to measure the Z_d polarization. However, when $\cos\theta_\ell \sim \pm 1$, one lepton is moving with the direction of motion of the Z_d in the lab frame and the other lepton in the opposite direction. The boost from the Z_d rest frame to the lab frame is then against the direction of motion of one of the leptons. Hence, this configuration results in events with the softest leptons, and the transverse momentum cut of Eq. (16) eliminates the events with $\cos\theta_\ell \sim \pm 1$. Since this region is vital in distinguishing between our two cases, it will be useful to use another angular distribution directly related to that of Eq. (24).

In the partonic center of momentum (c.m.) frame, the Z and Z_d momentum and spin must be antialigned by conservation of momentum and angular momentum, respectively. As a result, if the Z_d is in a helicity eigenstate, then in the partonic c.m. the Z is also in the same helicity eigenstate. The angular distribution of Z decay products will be of the same form as Eq. (24), now with the angle measured in the Z rest frame with respect to the Z moving direction in the partonic c.m. frame. Since the decay products of the Z are typically harder than those of the Z_d, the p_T cuts are not severe, and the angular distribution is a good diagnostic of the Z_d polarization.

In Fig. 7, we show the simulated angular distribution of the lepton identified as originating from the Z decay for operators of class (A) (solid black) and class (B) (solid red/grey) and the expected distributions for longitudinally and transversely polarized Z_d (dashed black and red/grey, respectively). Both operators of class (B), Eqs. (5) and (6), result in the same angular distributions as we take either $\kappa_Z \neq 0$, $\tilde{\kappa}_Z = 0$ or $\kappa_Z = 0$, $\tilde{\kappa}_Z \neq 0$. The CP violating effect would show up as an interference effect when both operators are present. Note that for $\delta = 0$, the values of κ_Z and $\tilde{\kappa}_Z$ will effect the total rate of our process but not the distributions in Fig. 7, since they have been normalized.

These angular distributions are measured in the reconstructed Z rest frame with respect to the Z moving direction in the partonic c.m. frame. As can be seen in Fig. 7(a), without energy smearing or cuts it is clear that, using the above definition, the angular distribution of the Z decay products reflect the expected Z_d polarization. That is, operators of class (A) result in events that are dominated by

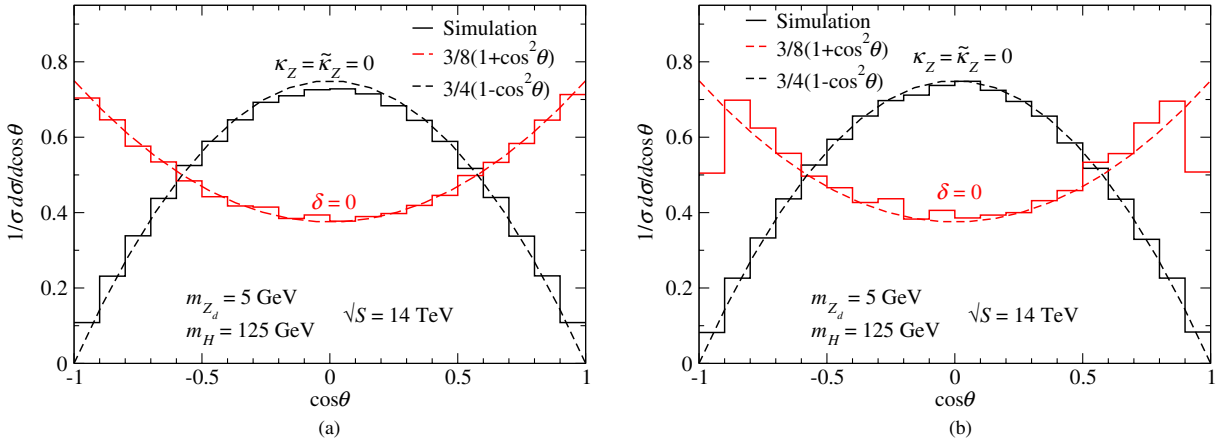

FIG. 7 (color online). Solid histograms are event simulation results for angular distributions of the ℓ^- identified as originating from the Z in the reconstructed Z rest frame (a) without cuts or smearing and (b) with energy smearing, triggers, and cuts from Eqs. (16)–(23). The angle is measured with respect to the Z moving direction in the partonic c.m. frame. Dashed lines are expected distribution for longitudinally (black) and transversely (red/grey) polarized Z_d's.

longitudinal Z's and Z_d's, while the operators of class (B) are dominated by transversely polarized Z's and Z_d's.

Figure 7(b) illustrates the effects of the cuts on the angular distributions. Even after cuts, the two distributions are still clearly distinguishable. The small relative depletion of events at $\cos\theta_\ell \sim \pm 1$ is due to the isolation cuts in Eq. (17). This can be understood by noting that for $\cos\theta_\ell \sim \pm 1$ in the Z rest frame, one lepton from the Z decay is moving directly against the Z moving direction in the partonic c.m. frame. Also, since $m_Z \sim m_H$, the Z is produced nearly at threshold, and its decay products move back-to-back in the partonic c.m. frame. Hence, for $\cos\theta_\ell \sim \pm 1$, one of the leptons from Z decay is typically moving in the Z_d direction. In this configuration, ΔR between the Z and Z_d decay products is minimized and fails the cut in Eq. (17).

V. CONCLUSIONS

Recent data from the LHC appears to have uncovered a Higgs scalar associated with the mechanism responsible for spontaneous electroweak symmetry breaking. The new scalar H may exhibit properties that lead to deviations from the SM predictions. Early findings suggest inconclusive yet tantalizing hints for such deviations in Higgs decays. Regardless of the fate of these hints, searching for physics beyond the SM is well motivated, especially in light of the need to account for the cosmic dark matter density in the Universe. It is reasonable to expect that the dark or hidden sector of particle physics, like its visible counterpart, is endowed with structure and its own forces. In fact, certain astrophysical observations have been interpreted as signals of dark matter that couples to a hidden sector light vector boson. One can then ask whether the forces in the dark sector could manifest themselves through their interactions with the Higgs.

Based on the above motivation, in this work we have studied the possibility that a dark vector boson Z_d, in the mass range of 5–10 GeV, could couple to H via mixing or through loop effects. These couplings can then be described by two classes of operators, leading to Higgs decays into dominantly longitudinal or transverse Z_d. An interesting typical decay in the first class is $H \to ZZ_d$, while the second class of decays could include $H \to XZ_d$, with $X = Z, Z_d, \gamma$.

We focused on $H \to ZZ_d$, as a representative novel decay channel. Using leptonic final states for both Z and Z_d, we found that the next run of the LHC is capable of excluding or detecting such decays for $\delta^2 \times \mathrm{Br}(Z_d \to \ell^+\ell^-) \sim 10^{-5}$ and $m_{Z_d} \sim 5$–10 GeV or loop induced dimension-5 operators of similar magnitude, with a few hundred fb^{-1} of data. The branching ratios of Z_d in leptons can be as large as $\mathrm{Br}(Z_d \to e^+e^-) \simeq \mathrm{Br}(Z_d \to \mu^+\mu^-) \simeq 0.15$. For somewhat lower m_{Z_d}, larger backgrounds will probably require longer running. These LHC searches via rare Higgs decays provide a complementary approach to low energy experiments that are primarily sensitive to dark vector boson masses at or below the GeV scale.

Our results also suggest that one could use the angular distribution of the leptons from the Z in $H \to ZZ_d$ to probe the underlying microphysical interaction. Those distinct distributions can be used to determine whether the Z_d emitted in the decay was longitudinal or transverse, providing a probe of the nature of the Higgs coupling to the dark sector.

In the various scenarios we have considered, the Higgs boson can also decay into γZ_d and Z_dZ_d. Although we have not discussed those modes in detail here, they entail very distinct signatures [22] that should help separate them from background and ordinary SM Higgs decays. For example, in the case of very light final state Z_d bosons, they look like promptly converted e^+e^- photons; a feature that distinguishes them from ordinary diphoton events. Heavier Z_d decays could stand out above Dalitz and four lepton ordinary decays of the Higgs, depending on their abundance in the data.

We hope that our work encourages further examination of the Higgs properties at the LHC, or future facilities, as a potential means of peering into the hidden sector and shedding light on the nature of dark matter or other as yet unknown phenomena.

ACKNOWLEDGMENTS

We would like to thank Jay Hubisz for useful discussions and Bogdan Wojtsekhowski for useful comments. This work was supported in part by the United States DOE under Grants No. DE-AC02-98CH10886 and No. DE-AC05-06OR23177 and by the NSF under Grant No. PHY-1068008. W. M. acknowledges partial support as a Fellow in the Gutenberg Research College.

APPENDIX: VARIOUS RELEVANT HIGGS DECAY WIDTHS

1. $H \to ZZ_d$ decay

The amplitude for $H \to Z(p)Z_d(q)$ is

$$i\mathcal{M} = i\mathcal{C}^{\rm SM}_{HZZ} K_{ZZ_d,\mu\nu}\epsilon^{*\nu}(p)\epsilon^{*\mu}(q), \tag{A1}$$

where $\mathcal{C}^{\rm SM}_{HZZ} \equiv g m_Z/\cos\theta_W$ is the SM HZZ coupling and

$$K_{ZZ_d,\mu\nu} = \left(\varepsilon_Z g_{\mu\nu} + \frac{\kappa}{m_Z^2}(p\cdot q g_{\mu\nu} - p_\mu q_\nu) + \frac{\tilde\kappa}{m_Z^2}\varepsilon_{\mu\nu\rho\sigma}p^\rho q^\sigma\right). \tag{A2}$$

Here, tree-level mixing (ε_Z) is from dimension-3 operators [Eq. (9)] and loop-induced couplings (κ_Z for the CP conserving part and $\tilde\kappa_Z$ for the CP violating part) is from dimension-5 operators [Eqs. (10) and (11)].

We obtain, after summing over polarizations,

$$\sum_{\rm pol}|\mathcal{M}|^2 = (\mathcal{C}^{\rm SM}_{HZZ})^2\left[\varepsilon_Z^2\left(\frac{(p\cdot q)^2}{m_Z^2 m_{Z_d}^2}+2\right) + 6\varepsilon_Z\frac{\kappa_Z}{m_Z^2}(p\cdot q) + \left(\frac{\kappa_Z}{m_Z^2}\right)^2(m_Z^2 m_{Z_d}^2 + 2(p\cdot q)^2) - 2\left(\frac{\tilde\kappa_Z}{m_Z^2}\right)^2(m_Z^2 m_{Z_d}^2 - (p\cdot q)^2)\right], \tag{A3}$$

with $p\cdot q = \frac{1}{2}(m_H^2 - m_Z^2 - m_{Z_d}^2)$ for $H \to ZZ_d$ decay.

For $m_{Z_d}^2 \ll D^2$ (with $D^2 \equiv m_H^2 - m_Z^2$), we have

$$\Gamma(H\to ZZ_d) = 4\pi\frac{\sqrt{\lambda(m_H^2, m_Z^2, m_{Z_d}^2)}}{64\pi^2 m_H^3}\sum_{\rm pol}|\mathcal{M}|^2 \tag{A4}$$

$$\simeq \frac{D^2}{16\pi m_H^3}(\mathcal{C}^{\rm SM}_{HZZ})^2\left(\varepsilon_Z^2\frac{D^4}{4m_Z^2 m_{Z_d}^2} + 3\varepsilon_Z\kappa_Z\frac{D^2}{m_Z^2} + \kappa_Z^2\frac{D^4}{2m_Z^4} + \tilde\kappa_Z^2\frac{D^4}{2m_Z^4}\right), \tag{A5}$$

with $\lambda(x,y,z) = x^2+y^2+z^2-2xy-2yz-2zx$.

As expected, the longitudinal polarization limit (κ_Z, $\tilde\kappa_Z \to 0$) shows an enhancement as $m_{Z_d} \to 0$, in accordance with the Goldstone boson equivalence theorem, while the transverse polarization limit ($\varepsilon_Z \to 0$) does not. However, because $\varepsilon_Z = \delta m_{Z_d}/m_Z$, the rate is not singular.

2. $H \to Z_d Z_d$ decay

The amplitude for the decay $H \to Z_d(p)Z_d(q)$ is given by

$$i\mathcal{M} = i\mathcal{C}^{\rm SM}_{HZZ} K_{Z_dZ_d,\mu\nu}\epsilon^{*\nu}(p)\epsilon^{*\mu}(q). \tag{A6}$$

When operators of class (A) arise from Z-Z_d mass mixing, two insertions of the mixing angle are needed to obtain a H-Z_d-Z_d coupling. This is equivalent to the replacement $\varepsilon_Z \to \varepsilon_Z^2$. Since operators of class (B) arise from loops, the H-Z_d-Z_d and H-Z-Z_d interactions are of the same form in this case. The effective Feynman rule for the H-Z_d-Z_d coupling is of the same form as the right-hand side of Eq. (A2) with $\varepsilon_Z \to \varepsilon_Z^2$, and we get

$$\sum_{\rm pol}|\mathcal{M}|^2 = (\mathcal{C}^{\rm SM}_{HZZ})^2\left[\varepsilon_Z^4\left(\frac{(p\cdot q)^2}{m_{Z_d}^4}+2\right) + 6\varepsilon_Z^2\frac{\kappa_{Z_d}}{m_Z^2}(p\cdot q) + \left(\frac{\kappa_{Z_d}}{m_Z^2}\right)^2(m_{Z_d}^4 + 2(p\cdot q)^2) - 2\left(\frac{\tilde\kappa_{Z_d}}{m_Z^2}\right)^2(m_{Z_d}^4 - (p\cdot q)^2)\right], \tag{A7}$$

with $p\cdot q = \frac{1}{2}(m_H^2 - 2m_{Z_d}^2)$ for $H \to Z_dZ_d$ decay. For the case of scalar mixing in the Higgs sector, see Ref. [17].

For $m_{Z_d}^2 \ll D^2$ (with $D^2 \equiv m_H^2$), we have

$$\Gamma(H\to Z_dZ_d) = \frac{4\pi}{2}\frac{\sqrt{\lambda(m_H^2, m_{Z_d}^2, m_{Z_d}^2)}}{64\pi^2 m_H^3}\sum_{\rm pol}|\mathcal{M}|^2 \tag{A8}$$

$$\simeq \frac{D^2}{32\pi m_H^3}(\mathcal{C}^{\rm SM}_{HZZ})^2\left(\varepsilon_Z^4\frac{D^4}{4m_{Z_d}^4} + 3\varepsilon_Z^2\kappa_{Z_d}\frac{D^2}{m_Z^2} + \kappa_{Z_d}^2\frac{D^4}{2m_Z^4} + \tilde\kappa_{Z_d}^2\frac{D^4}{2m_Z^4}\right). \tag{A9}$$

3. $H \to \gamma Z_d$ decay

The amplitude for $H \to \gamma(p)Z_d(q)$ is given by

$$i\mathcal{M} = i\mathcal{C}^{\rm SM}_{HZZ} K_{\gamma Z_d,\mu\nu}\epsilon^{*\nu}(p)\epsilon^{*\mu}(q), \tag{A10}$$

with the effective Feynman rule of H-γ-Z_d coupling being the same form as in the right-hand side of Eq. (A2), except that there is no ε_Z term here.

We then have

$$\sum_{\rm pol}|\mathcal{M}|^2 = 2(\mathcal{C}^{\rm SM}_{HZZ})^2(\kappa_\gamma^2 + \tilde\kappa_\gamma^2)\left(\frac{p\cdot q}{m_Z^2}\right)^2, \tag{A11}$$

with $p\cdot q = \frac{1}{2}(m_H^2 - m_{Z_d}^2)$ for $H \to \gamma Z_d$ decay.

For $m_{Z_d}^2 \ll D^2$ (with $D^2 \equiv m_H^2$), we obtain

$$\Gamma(H \to \gamma Z_d) = 4\pi \frac{\sqrt{\lambda(m_H^2, 0, m_{Z_d}^2)}}{64\pi^2 m_H^3} \sum_{\text{pol}} |\mathcal{M}|^2 \tag{A12}$$

$$\simeq \frac{1}{32\pi} (C_{HZZ}^{\text{SM}})^2 \frac{D^6}{m_H^3 m_Z^4} (\kappa_\gamma^2 + \tilde{\kappa}_\gamma^2). \tag{A13}$$

As expected, there is no enhancement from the longitudinal polarization of Z_d in this case.

[1] G. Aad *et al.* (ATLAS Collaboration), Phys. Lett. B **716**, 1 (2012).
[2] S. Chatrchyan *et al.* (CMS Collaboration), Phys. Lett. B **716**, 30 (2012).
[3] J. R. Ellis, M. K. Gaillard, and D. V. Nanopoulos, Nucl. Phys. **B106**, 292 (1976).
[4] M. A. Shifman, A. I. Vainshtein, M. B. Voloshin, and V. I. Zakharov, Yad. Fiz. **30**, 1368 (1979) [Sov. J. Nucl. Phys. **30**, 711 (1979)].
[5] ATLAS Collaboration, ATLAS-CONF-2013-012; CMS Collaboration, CMS-PAS-HIG-13-001.
[6] J. Beringer *et al.* (Particle Data Group Collaboration), Phys. Rev. D **86**, 010001 (2012).
[7] C. Boehm and P. Fayet, Nucl. Phys. **B683**, 219 (2004).
[8] C. Boehm, D. Hooper, J. Silk, M. Casse, and J. Paul, Phys. Rev. Lett. **92**, 101301 (2004).
[9] C. Boehm, P. Fayet, and J. Silk, Phys. Rev. D **69**, 101302 (2004).
[10] P. Jean *et al.*, Astron. Astrophys. **407**, L55 (2003).
[11] N. Arkani-Hamed, D. P. Finkbeiner, T. R. Slatyer, and N. Weiner, Phys. Rev. D **79**, 015014 (2009).
[12] J. Chang *et al.*, Nature (London) **456**, 362 (2008).
[13] O. Adriani *et al.* (PAMELA Collaboration), Nature (London) **458**, 607 (2009).
[14] G. W. Bennett *et al.* (Muon G-2 Collaboration), Phys. Rev. D **73**, 072003 (2006).
[15] A. Czarnecki and W. J. Marciano, Phys. Rev. D **64**, 013014 (2001).
[16] A. Y. Korchin and V. A. Kovalchuk, arXiv:1303.0365.
[17] S. Gopalakrishna, S. Jung, and J. D. Wells, Phys. Rev. D **78**, 055002 (2008).
[18] H. Davoudiasl, H.-S. Lee, and W. J. Marciano, Phys. Rev. D **85**, 115019 (2012).
[19] J. M. Cornwall, D. N. Levin, and G. Tiktopoulos, Phys. Rev. D **10**, 1145 (1974); **11**, 972(E) (1975); M. S. Chanowitz and M. K. Gaillard, Nucl. Phys. **B261**, 379 (1985); W. J. Marciano and S. S. D. Willenbrock, Phys. Rev. D **37**, 2509 (1988).
[20] H. Davoudiasl, H.-S. Lee, and W. J. Marciano, Phys. Rev. Lett. **109**, 031802 (2012).
[21] K. S. Kumar, S. Mantry, W. J. Marciano, and P. A. Souder, arXiv:1302.6263.
[22] H. Davoudiasl, H.-S. Lee, and W. J. Marciano, Phys. Rev. D **86**, 095009 (2012).
[23] M. B. Voloshin, Phys. Rev. D **86**, 093016 (2012).
[24] B. Holdom, Phys. Lett. **166B**, 196 (1986).
[25] Some recent works that employ kinetic mixing between the Standard Model and dark gauge sector include Ref. [17] and the following: M. Pospelov, Phys. Rev. D **80**, 095002 (2009); M. Reece and L.-T. Wang, J. High Energy Phys. 07 (2009) 051; J. D. Bjorken, R. Essig, P. Schuster, and N. Toro, Phys. Rev. D **80**, 075018 (2009); A. Hook, E. Izaguirre, and J. G. Wacker, Adv. High Energy Phys. **2011**, 859762 (2011); Y. Mambrini, J. Cosmol. Astropart. Phys. 09 (2010) 022; 07 (2011) 009; A. Alves, E. Ramirez Barreto, A. G. Dias, C. A. de S Pires, F. S. Queiroz, and P. S. Rodrigues da Silva, Phys. Rev. D **84**, 115004 (2011); A. Alves, A. G. Dias, E. Ramirez Barreto, C. A. de S Pires, F. S. Queiroz, and P. S. Rodrigues da Silva, Eur. Phys. J. C **73**, 2288 (2013).
[26] For discussions of non-Abelian dark gauge sectors, see M. Baumgart, C. Cheung, J. T. Ruderman, L.-T. Wang, and I. Yavin, J. High Energy Phys. 04 (2009) 014; F. Chen, J. M. Cline, and A. R. Frey, Phys. Rev. D **80**, 083516 (2009); H. Zhang, C. S. Li, Q.-H. Cao, and Z. Li, Phys. Rev. D **82**, 075003 (2010); C. D. Carone, Phys. Lett. B **721**, 118 (2013).
[27] P. Fayet, Phys. Rev. D **75**, 115017 (2007).
[28] M. Pospelov, Phys. Rev. D **80**, 095002 (2009).
[29] M. Endo, K. Hamaguchi, and G. Mishima, Phys. Rev. D **86**, 095029 (2012).
[30] J. D. Bjorken, R. Essig, P. Schuster, and N. Toro, Phys. Rev. D **80**, 075018 (2009).
[31] S. Andreas, C. Niebuhr, and A. Ringwald, Phys. Rev. D **86**, 095019 (2012).
[32] D. Babusci *et al.* (KLOE-2 Collaboration), Phys. Lett. B **720**, 111 (2013).
[33] R. Meijer Drees *et al.* (SINDRUM I Collaboration), Phys. Rev. Lett. **68**, 3845 (1992).
[34] S. N. Gninenko, Phys. Rev. D **87**, 035030 (2013).
[35] P. Adlarson *et al.* (WASA-at-COSY Collaboration), arXiv:1304.0671.
[36] H. Merkel *et al.* (A1 Collaboration), Phys. Rev. Lett. **106**, 251802 (2011).
[37] S. Abrahamyan *et al.* (APEX Collaboration), Phys. Rev. Lett. **107**, 191804 (2011).
[38] R. D. McKeown, AIP Conf. Proc. **1423**, 289 (2012).
[39] S. Dawson and E. Furlan, Phys. Rev. D **86**, 015021 (2012).

[40] M. Carena, I. Low, and C. E. M. Wagner, J. High Energy Phys. 08 (2012) 060.

[41] N. Bonne and G. Moreau, Phys. Lett. B **717**, 409 (2012).

[42] H. An, T. Liu, and L.-T. Wang, Phys. Rev. D **86**, 075030 (2012).

[43] A. Joglekar, P. Schwaller, and C. E. M. Wagner, J. High Energy Phys. 12 (2012) 064.

[44] N. Arkani-Hamed, K. Blum, R. T. D'Agnolo, and J. Fan, J. High Energy Phys. 01 (2013) 149.

[45] L. G. Almeida, E. Bertuzzo, P. A. N. Machado, and R. Z. Funchal, J. High Energy Phys. 11 (2012) 085.

[46] J. Kearney, A. Pierce, and N. Weiner, Phys. Rev. D **86**, 113005 (2012).

[47] M. A. Ajaib, I. Gogoladze, and Q. Shafi, Phys. Rev. D **86**, 095028 (2012).

[48] S. Dawson, E. Furlan, and I. Lewis, Phys. Rev. D **87**, 014007 (2013).

[49] H. Davoudiasl, I. Lewis, and E. Ponton, Phys. Rev. D **87**, 093001 (2013).

[50] H.-S. Lee and M. Sher, Phys. Rev. D **87**, 115009 (2013).

[51] ATLAS Collaboration, Report No. ATLAS-CONF-2013-013.

[52] CMS Collaboration, Report No. CMS-PAS-HIG-13-002.

[53] K. Agashe, H. Davoudiasl, S. Gopalakrishna, T. Han, G.-Y. Huang, G. Perez, Z.-G. Si, and A. Soni, Phys. Rev. D **76**, 115015 (2007).

[54] V. Barger, P. Langacker, and H.-S. Lee, Phys. Rev. Lett. **103**, 251802 (2009).

[55] J. Alwall, M. Herquet, F. Maltoni, O. Mattelaer, and T. Stelzer, J. High Energy Phys. 06 (2011) 128.

[56] J. Pumplin, D. R. Stump, J. Huston, H. L. Lai, P. M. Nadolsky, and W. K. Tung, J. High Energy Phys. 07 (2002) 012.

[57] N. D. Christensen and C. Duhr, Comput. Phys. Commun. **180**, 1614 (2009).

[58] *The CERN Large Hadron Collider, Accelerator and Experiments,*, edited by R. Voss and A. Breskin (CERN, Geneva, 2009).

[59] W.-Y. Keung and W. J. Marciano, Phys. Rev. D **30**, 248 (1984).

[60] R. V. Harlander and W. B. Kilgore, Phys. Rev. Lett. **88**, 201801 (2002).

[61] C. Anastasiou and K. Melnikov, Nucl. Phys. **B646**, 220 (2002); V. Ravindran, J. Smith, and W. L. van Neerven, Nucl. Phys. **B665**, 325 (2003); S. Catani, D. de Florian, M. Grazzini, and P. Nason, J. High Energy Phys. 07 (2003) 028; V. Ahrens, T. Becher, M. Neubert, and L. L. Yang, Phys. Rev. D **79**, 033013 (2009); Eur. Phys. J. C **62**, 333 (2009).

[62] M. Czakon, P. Fiedler, and A. Mitov, arXiv:1303.6254.

[63] R. Hamberg, W. L. van Neerven, and T. Matsuura, Nucl. Phys. **B359**, 343 (1991); **B644**, 403(E) (2002); C. Anastasiou, L. J. Dixon, K. Melnikov, and F. Petriello, Phys. Rev. Lett. **91**, 182002 (2003); Phys. Rev. D **69**, 094008 (2004); K. Melnikov and F. Petriello, Phys. Rev. D **74**, 114017 (2006); S. Catani, L. Cieri, G. Ferrera, D. de Florian, and M. Grazzini, Phys. Rev. Lett. **103**, 082001 (2009).

[64] J. M. Campbell, R. K. Ellis, and C. Williams, J. High Energy Phys. 07 (2011) 018.

[65] J. Ohnemus, Phys. Rev. D **47**, 940 (1993); U. Baur, T. Han, and J. Ohnemus, Phys. Rev. D **57**, 2823 (1998); D. De Florian and A. Signer, Eur. Phys. J. C **16**, 105 (2000).

[66] J. Ohnemus and J. F. Owens, Phys. Rev. D **43**, 3626 (1991); B. Mele, P. Nason, and G. Ridolfi, Nucl. Phys. **B357**, 409 (1991); T. Matsuura and J. J. van der Bij, Z. Phys. C **51**, 259 (1991); J. Ohnemus, Phys. Rev. D **50**, 1931 (1994); L. J. Dixon, Z. Kunszt, and A. Signer, Nucl. Phys. **B531**, 3 (1998); Phys. Rev. D **60**, 114037 (1999).

[67] J. M. Campbell, R. K. Ellis, and D. L. Rainwater, Phys. Rev. D **68**, 094021 (2003); C. F. Berger, Z. Bern, L. J. Dixon, F. Febres Cordero, D. Forde, T. Gleisberg, H. Ita, D. A. Kosower, and D. Maître, Phys. Rev. D **82**, 074002 (2010).

[68] B. Wojtsekhowski, D. Nikolenko, and I. Rachek, arXiv:1207.5089.